AB-Cache: Training-Free Acceleration of Diffusion Models via Adams-Bashforth Cached Feature Reuse

Zichao Yu [*1], Zhen Zou[1], Guojiang Shao [†2], Chengwei Zhang[1], Shengze Xu[3], Jie Huang[1], Feng Zhao[1], Xiaodong Cun[4], and Wenyi Zhang[‡1]

[1]University of Science and Technology of China, Hefei, China
[2]Fudan University, Shanghai, China
[3]The Chinese university of HongKong, HongKong, China
[4]Great Bay University, Dongguan, China

Abstract

Diffusion models have demonstrated remarkable success in generative tasks, yet their iterative denoising process results in slow inference, limiting their practicality. While existing acceleration methods exploit the well-known U-shaped similarity pattern between adjacent steps through caching mechanisms, they lack theoretical foundation and rely on simplistic computation reuse, often leading to performance degradation. In this work, we provide a theoretical understanding by analyzing the denoising process through the second-order Adams-Bashforth method, revealing a linear relationship between the outputs of consecutive steps. This analysis explains why the outputs of adjacent steps exhibit a U-shaped pattern. Furthermore, extending Adams-Bashforth method to higher order, we propose a novel caching-based acceleration approach for diffusion models, instead of directly reusing cached results, with a truncation error bound of only $O(h^k)$ where h is the step size. Extensive validation across diverse image and video diffusion models (including HunyuanVideo and FLUX.1-dev) with various schedulers demonstrates our method's effectiveness in achieving nearly 3× speedup while maintaining original performance levels, offering a practical real-time solution without compromising generation quality.

Keywords:Adams-Bashforth method, Caching-based acceleration approach, Diffusion model, Linear approximation relationship, Training-free

1 Introduction

In recent years, diffusion models (Ho et al., 2020; Song and Ermon, 2019; Song et al., 2020b) have emerged as a powerful framework in generative tasks, owing to their exceptional ability to generate high-quality, diverse outputs with strong theoretical underpinnings. These models excel in capturing intricate data distributions (Song et al., 2021), making them highly effective for applications such as image synthesis (Chen et al., 2023; Rombach et al., 2022), audio generation (Liu et al., 2024a; Tian et al., 2025), and text-to-video tasks (HaCohen et al., 2024; Kong et al., 2024; Yang et al., 2024). Architecturally, diffusion models have evolved significantly, transitioning from the foundational U-Net backbone to the more advanced Diffusion Transformer (DiT) (Peebles and Xie, 2023), which incorporates transformer-based architectures (Vaswani et al., 2017) for improved

---

[*]zichaoyu@mail.ustc.edu.cn

[†]gjshao@m.fudan.edu.cn

[‡]wenyizha@ustc.edu.cn

scalability and performance. Notable examples of their application include DALL·E 2 and Stable Diffusion for efficient and photorealistic text-to-image synthesis. However, despite these strengths, a key drawback of diffusion models is their slow inference speed, which stems from the iterative denoising process, limiting their practicality for large-scale, real-time applications.

To address this challenge, recent research has broadly categorized methods for accelerating diffusion model inference into two main approaches: reducing the number of sampling steps and lowering the inference cost per sampling step. The first category focuses on designing advanced probabilistic flow Ordinary Differential Equation (ODE) solvers or employing distillation techniques to condense the denoising trajectory into fewer steps. Methods in the second branch primarily focus on compressing the model size (Kim et al., 2023) or utilizing low-precision data formats (Li et al., 2023c). A novel approach for dynamically adjusting the computation process in diffusion models introduces a specialized caching mechanism during the denoising process (Li et al., 2023a; Ma et al., 2024a). This method capitalizes on the high similarity between consecutive steps and the unique properties of U-Net or DiT to cache intermediate computations, which are then efficiently reused in subsequent steps. Alternatively, certain dynamic inference strategies utilize a range of diffusion models, assigning specialized networks to individual steps (Li et al., 2023b; Liu et al., 2023a).

Despite the proven effectiveness of caching-based acceleration methods for diffusion model inference, two critical concerns remain: 1) The high similarity of certain features observed during the denoising process is primarily experimental, lacking solid theoretical analysis. 2) Current caching mechanisms mainly focus on identifying which modules exhibit higher feature similarity or determining the specific steps where caching should be applied, followed by simply reusing the previously cached computation results. To close this gap, this paper addresses both concerns by providing a theoretical foundation for the observed feature similarities and proposing a simpler but efficient caching mechanism that goes beyond simply reusing previously cached computation results.

Current literature on caching-based acceleration for diffusion models has experimentally observed a U-shaped phenomenon during the inference process. Unlike previous works (Shen et al., 2024), which analyze the lower bound of similarity between outputs at consecutive steps and highlight its notably high value, we adopt a numerical integration-based approach. By examining the integral equations underlying the denoising process in diffusion models, we provide a fresh perspective to address this phenomenon. Rather than focusing on the properties of local modules within the network, we treat the network as a whole. Leveraging the second-order Adams-Bashforth method, we discover that the outputs of adjacent steps not only exhibit strong similarity but also follow a linear relationship. Inspired by this insight, we propose a novel yet simple and effective method to accelerate the inference process of diffusion models in a training-free manner, independent of the network architecture. Specifically, by introducing a caching mechanism during the denoising process, rather than merely reusing cached computation results, we perform a binomial combination of the cached results from the previous k steps. This approach achieves significant acceleration through a straightforward linear operation, all without compromising the quality of the generated outputs, with a truncation error of only $O(h^k)$, where h is the step size.

We evaluate the effectiveness of our method across a wide range of diffusion models, spanning from image diffusion models to video diffusion models. Experimental results demonstrate that our method achieves significant improvements in inference speed while maintaining comparable performance to the base model without acceleration.

In summary, our contributions are as follows:

- Our method establishes a theoretical foundation for the observed feature similarities in diffusion models. By employing numerical integration techniques, we not only confirm the high similarity between adjacent steps but also reveal a linear relationship governing their outputs during the denoising process.

- We propose a training-free and architecture-agnostic approach to accelerate diffusion model

inference. By leveraging a caching mechanism and a simple linear operation, our method significantly reduces computational costs while maintaining high-quality generation.

- Our method is extensively evaluated on a wide range of diffusion models, achieving state-of-the-art results in inference speed without sacrificing quality.

2 Related Works

Diffusion probability models (Ho et al., 2020; Song and Ermon, 2019; Song et al., 2020b) have achieved remarkable success in generative tasks, initially excelling in image synthesis (Chen et al., 2023; Ramesh et al., 2022; Rombach et al., 2022) through their ability to model complex data distributions via a gradual denoising process. Early architectures, such as UNet (Ronneberger et al., 2015), played a pivotal role in this success, leveraging encoder-decoder structures and skip connections to capture both local and global features, which proved essential for generating high-quality images. However, the intrinsic scalability limitations of the UNet architecture have posed challenges for large-scale and high-performance models. To address these challenges, the Diffusion Transformer (DiT) (Peebles and Xie, 2023) architecture has emerged as a promising solution. DiT harnesses the strengths of transformer-based (Vaswani et al., 2017) models, renowned for their scalability and ability to handle large-scale data, significantly enhancing the potential of diffusion models (Ma et al., 2024b; Yang et al., 2024; Zheng et al., 2024).
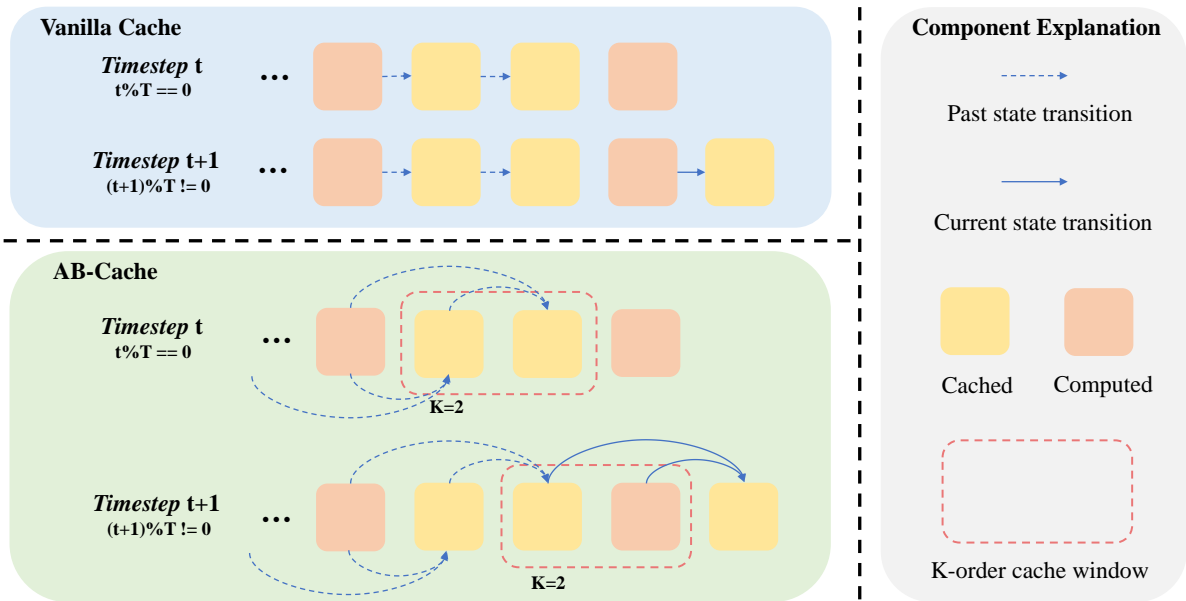
Figure 1: Similar to the base model, our method computes at timesteps where $t\%T == 0$ and caches states otherwise. However, we replace simple assignment with k-th order Adams-Bashforth numerical integration within the cache window, achieving more accurate state transitions while maintaining efficiency, as demonstrated in the K=2 case.

Despite the remarkable success of diffusion models in image and video generation, their widespread application has been significantly hindered by the substantial computational costs associated with inference. Current research on accelerating diffusion models primarily focuses on two key approaches: reducing the number of sampling steps and minimizing the computational cost of each sampling step.

Reduction of Sampling Steps. The core idea behind this line of work is to maintain high generation quality while significantly reducing the number of sampling steps. Many approaches

achieve this by employing efficient Stochastic Differential Equation (SDE) or ODE solvers. For instance, DDIM (Song et al., 2020a) introduced a non-Markovian process that enables faster sampling with fewer steps, while DPM-Solver (Karras et al., 2022; Lu et al., 2022a,b) optimized the sampling trajectory using advanced numerical methods. Another direction involves distilling the ODE trajectory of the diffusion sampling process into another neural network that enables fewer-step sampling. Methods like Progressive Distillation (Salimans and Ho, 2022) and its variants (Geng et al., 2023; Liu et al., 2023b; Meng et al., 2023; Sauer et al., 2024; Song et al., 2023) compress the denoising process into fewer steps, significantly reducing inference time.

Reducing Per-Step Cost. In addition to reducing the number of sampling steps, minimizing the computational cost of each sampling step is another promising approach to accelerating diffusion model inference. These methods can be broadly categorized into two classes: traditional model compression and quantization techniques, and caching-based acceleration methods for diffusion inference.

Model Compression and Quantization. Model compression techniques, such as pruning (Dong et al., 2017; Lee et al., 2019; Liu et al., 2021), reduce computational overhead by eliminating less important parts of the model, thereby decreasing inference latency. Similarly, quantization (Bhalgat et al., 2020; Gu et al., 2022; Li et al., 2023c; Shang et al., 2023) achieves this by representing model weights and activations with lower bit precision. However, these methods typically require additional training efforts to fine-tune the model and maintain the generation quality of diffusion models. While effective, this extra training overhead makes it challenging to apply these techniques to large, state-of-the-art models, especially in scenarios with limited computational resources. As a result, alternative approaches, such as caching-based acceleration or architectural optimizations, are often explored to achieve efficient inference without extensive retraining.

Caching-based Acceleration. Caching-Based Acceleration, a particularly relevant line of work exploits temporal redundancy in the diffusion process by reusing intermediate features between adjacent timesteps. Methods like TGATE (Zhang et al., 2024) cache and reuse attention outputs at scheduled timesteps, while DeepCache (Ma et al., 2024a) and Faster Diffusion (Li et al., 2023a) leverage feature caching mechanisms to indirectly modify the UNet diffusion process, thereby achieving enhanced acceleration. Building on these advancements, recent efforts have extended caching-based acceleration to Diffusion Transformer (DiT). For instance, Δ-DiT (Chen et al., 2024) caches the residuals between DiT blocks, and PAB (Zhao et al., 2024) caches and broadcasts intermediate computations at different timestep intervals based on the characteristics of varying attention output. FasterCache (Lv et al., 2024) accelerates diffusion-based video generation by leveraging a Dynamic Feature Reuse Strategy and exploiting redundancy in the classifier-free guidance (CFG). These approaches align closely with our work, as they leverage temporal redundancy to reduce computational overhead.

3 Methodology

3.1 Preliminary

In this subsection, we first review the fundamental concepts of diffusion probability models and their reverse processes.

Diffuison Model. Diffusion models are a class of generative models consisting of a forward diffusion process and a reverse generative process. The forward process progressively adds Gaussian noise to a data sample $\boldsymbol{x}_0 \sim p_{\text{data}}(\boldsymbol{x}_0)$, eventually destroying its structure. This process is formulated as:

$$q(\boldsymbol{x}_t|\boldsymbol{x}_0) = \mathcal{N}(\boldsymbol{x}_t; \sqrt{\alpha_t}\boldsymbol{x}_0, \sqrt{1 - \alpha_t}I),$$

where α_t represents a time-dependent noise schedule. Over time, this transformation converts the

data distribution into a Gaussian distribution as $t \to T$.

Regarding the reverse process, given two time steps s and t, where $s > 0$ and $t < s$, x_t is calculated as (Lu et al., 2022a):

$$\boldsymbol{x}_t = \frac{\alpha_t}{\alpha_s}\boldsymbol{x}_s - \alpha_t \int_{\lambda_s}^{\lambda_t} e^{-\lambda}\hat{\boldsymbol{\epsilon}}_\theta \left(\boldsymbol{x}_{t_\lambda(\lambda)}, t_\lambda(\lambda)\right) \mathrm{d}\lambda, \tag{3.1}$$

where $\lambda_t := \log\left(\alpha_t/\sigma_t\right)$, $t_\lambda(\lambda)$ is the inverse function of λ_t satisfying $t_\lambda(\lambda_t) = t$ and $\boldsymbol{\epsilon}_\theta(\cdot)$ often represents the learned model, which, in our case, is the diffusion transformer. Previous methods show that this integral term can be approximated by adopting Taylor expansion at λ_s, adopting the first-order or higher-order approximation (Lu et al., 2022a). Take the first-order one as an example, the update of $\boldsymbol{x}_t$ would be:

$$\boldsymbol{x}_t = \frac{\alpha_t}{\alpha_s}\boldsymbol{x}_s - \sigma_t \left(e^{\lambda_t - \lambda_s} - 1\right) \boldsymbol{\epsilon}_\theta\left(\boldsymbol{x}_s, s\right). \tag{3.2}$$

Adams-Bashforth Method. The Adams-Bashforth method (Butcher, 2016; Hairer, 1993) is a class of explicit linear multistep numerical techniques designed for solving ODEs. Introduced in the 19th century by John Couch Adams and Francis Bashforth, this method employs an iterative extrapolation strategy that leverages prior solution points to predict future values. It is particularly effective for non-stiff ODEs, offering superior accuracy compared to single-step methods such as Euler's approach, while significantly reducing computational overhead by minimizing redundant evaluations. A key advantage of the Adams-Bashforth method is its reliance on zero-order information—specifically, network outputs—without requiring higher-order derivatives or Taylor series expansions. This characteristic makes it both computationally efficient and straightforward to integrate into standard caching frameworks. In practice, lower-order variants of the method are predominantly used due to their simplicity and sufficient accuracy for most applications. As such, the subsequent discussion will focus primarily on these lower-order implementations, which are well-documented and widely referenced in numerical analysis literature.

3.2 Motivation: Rethinking Similarity in Diffusion Denoising Process

The denoising process in diffusion models is inherently iterative, requiring multiple steps to transform noisy inputs into high-quality outputs. A key observation in recent works (Ma et al., 2024a; Zhao et al., 2024) is the high similarity between intermediate computations across adjacent denoising steps, which has been empirically exploited to accelerate inference through caching mechanisms. Typically, this similarity is characterized by metrics that measure absolute differences, such as the relative L_p norm distance between feature vectors. So, it is natural to ask about the relationship between $\epsilon_\theta(\boldsymbol{x}_t, t)$ and $\epsilon_\theta(\boldsymbol{x}_s, s)$ for adjacent time steps t and s. Why do they perform so similarly? In this section, we provide a theoretical analysis to explore their relationship. Before presenting our conclusions, we conducted two preliminary experiments to validate the similarity between adjacent steps: one focusing on measuring value-based similarity, and the other on assessing directional similarity.

Our experiments reveal a more nuanced phenomenon: the similarity between steps is not only reflected in the magnitude of feature values but also in their directional alignment, as illustrated in Fig. 4. This directional similarity directly challenges the assumption that simply reusing cached computations from adjacent steps is an optimal strategy, as it ignores the structured evolution of features along a consistent trajectory.

To address this gap, we present a comprehensive theoretical analysis that treats the entire network as a unified entity, independent of specific architectural choices such as U-Net-based or DiT-based structures. This model-agnostic approach allows our analysis to generalize across diverse diffusion models, providing insights into the fundamental mechanisms driving the similarity in network outputs at adjacent time steps.
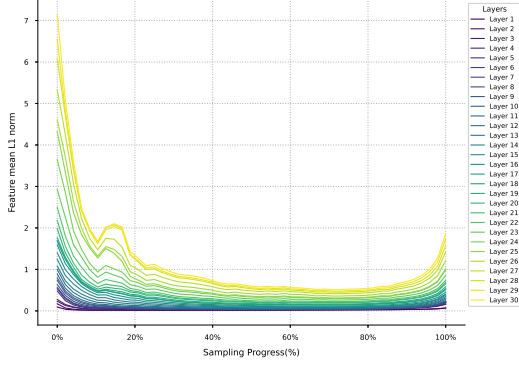
Figure 2: U-type similarity curve.
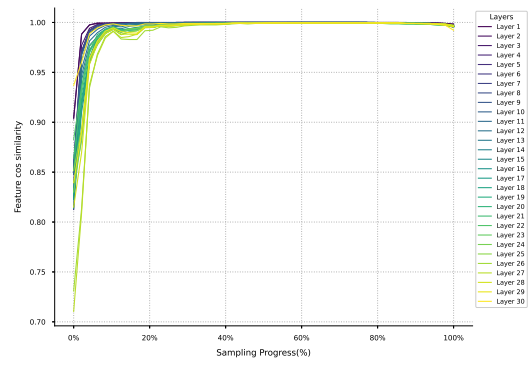
Figure 3: Directional consistency measured by cosine distance.

Figure 4: Analysis of U-type curve and directional consistency. Fig.2: U-type similarity curve, demonstrating high similarity between feature maps of adjacent steps; Fig.3: Directional consistency measured by cosine distance, validating the alignment of feature vectors.

3.3 U-Shaped Denoising Dynamics: An Adams-Bashforth Analysis of Diffusion Processes

Diffusion models learn to generate data by iteratively denoising samples through a reverse process, which is mathematically described as a reverse-time SDE. This reverse SDE is associated with a deterministic Probability Flow Ordinary Differential Equation, whose exact solution, as shown in Eq. (3.1), can be derived analytically. In this section, we leverage the Adams-Bashforth method to derive the relationship between the computational results at adjacent timesteps, effectively approximating future evaluations based on historical computations and further optimizing the inference efficiency. The integral of interest is defined as:

$$I = \int_{\lambda_s}^{\lambda_t} e^{-\lambda} \hat{\boldsymbol{\epsilon}}_\theta \left(\boldsymbol{x}_{t_\lambda(\lambda)}, t_\lambda(\lambda) \right) \mathrm{d}\lambda.$$

In order to approximate I numerically, heuristically, we take the second-order Adams-Bashforth (AB2) scheme to compute the vector-valued integral. Actually, we can get the following approximate relationship.

Proposition 1. *Let $h = \lambda_t - \lambda_s = \lambda_s - \lambda_o$ be step size, with some mild conditions the same as those in (Lu et al., 2022a), we can obtain:*

$$\hat{\boldsymbol{\epsilon}}_\theta \left(\boldsymbol{x}_{t_\lambda(\lambda_s)}, t_\lambda(\lambda_s) \right) = \frac{\alpha_t h}{3e^{-h}\alpha_t h - 2\sigma_{\lambda_t} e^{\lambda_o}(e^h - 1)} \hat{\boldsymbol{\epsilon}}_\theta \left(\boldsymbol{x}_{t_\lambda(\lambda_o)}, t_\lambda(\lambda_o) \right) + O(h^2). \tag{3.3}$$

Proof. Let $\boldsymbol{x}_t$ be a function satisfying the integral equation,

$$\boldsymbol{x}_t = \frac{\alpha_t}{\alpha_s} \boldsymbol{x}_s - \alpha_t \int_{\lambda_s}^{\lambda_t} e^{-\lambda} \hat{\boldsymbol{\epsilon}}_\theta \left(\boldsymbol{x}_{t_\lambda(\lambda)}, t_\lambda(\lambda) \right) \mathrm{d}\lambda, \tag{3.4}$$

where $\boldsymbol{x}_t, \boldsymbol{x}_s \in \mathbb{R}^n$ are vector-valued functions and $\hat{\boldsymbol{\epsilon}}_\theta : \mathbb{R}^n \times \mathbb{R} \to \mathbb{R}^n$ is a twice continuously differentiable function parameterized by θ. We also assume $t_\lambda(\lambda)$ is a continuous mapping from λ to time and λ_t is continuously differentiable twice. With Lagrange linear interpolation, we can approximate the integrand in equality (3.4) with the following linear function

$$p(u) := (u+1)e^{-\lambda_s} \hat{\boldsymbol{\epsilon}}_\theta \left(\boldsymbol{x}_{t_\lambda(\lambda_s)}, t_\lambda(\lambda_s) \right) - u e^{-\lambda_o} \hat{\boldsymbol{\epsilon}}_\theta \left(\boldsymbol{x}_{t_\lambda(\lambda_o)}, t_\lambda(\lambda_o) \right),$$

6

where

$$u = \frac{\lambda - \lambda_s}{h} \in [0, 1],$$

hence we are able to approximate I with the value of $h \int_0^1 p(u)\mathrm{d}u$, thus

$$I = h \left(\frac{3}{2} e^{-\lambda_s} \hat{\epsilon}_\theta \left(\boldsymbol{x}_{t_\lambda(\lambda_s)}, t_\lambda(\lambda_s) \right) - \frac{1}{2} e^{-\lambda_o} \hat{\epsilon}_\theta \left(\boldsymbol{x}_{t_\lambda(\lambda_o)}, t_\lambda(\lambda_o) \right) \right) + O(h^3). \tag{3.5}$$

With sufficiently small step size h, the integral I is approximated with $O(h^2)$ global error. On the other hand, according to Equation (3.2), we observe that:

$$\alpha_t I = \sigma_{\lambda_t} (e^h - 1) \hat{\epsilon}_\theta \left(\boldsymbol{x}_{t_\lambda(\lambda_s)}, t_\lambda(\lambda_s) \right) + O(h^2),$$

combining with Eq. (3.5), we can demonstrate the linear relationship of $\hat{\epsilon}_\theta \left(\boldsymbol{x}_{t_\lambda(\lambda_o)}, t_\lambda(\lambda_o) \right)$ and $\hat{\epsilon}_\theta \left(\boldsymbol{x}_{t_\lambda(\lambda_s)}, t_\lambda(\lambda_s) \right)$ as Equation (3.3) shows. $\qquad \square$

Based on the above proposition, we find that when the truncation error is $O(h^2)$, the network outputs of the diffusion model at adjacent time steps differ by a scaling factor, satisfying the linear relationship (3.3). The relationship between the network outputs at consecutive time steps can be expressed as *coefficient* $r = \frac{\alpha_t h}{3e^{-h}\alpha_t h - 2\sigma_{\lambda_t} e^{\lambda_o}(e^h - 1)}$, within the tolerance of second-order error. In other words, given the initial values, r determines the trend of changes in the network outputs between adjacent time steps. The variation curve of the scale factor is shown in Fig. 5. As can be seen from the curve in the figure, the coefficient is around 1 during the middle period, while it deviates from 1 at the beginning and the end. This pattern aligns with the U-shaped curve commonly observed in (Lv et al., 2024; Ma et al., 2024a)on caching-based accelerating diffusion model inference.
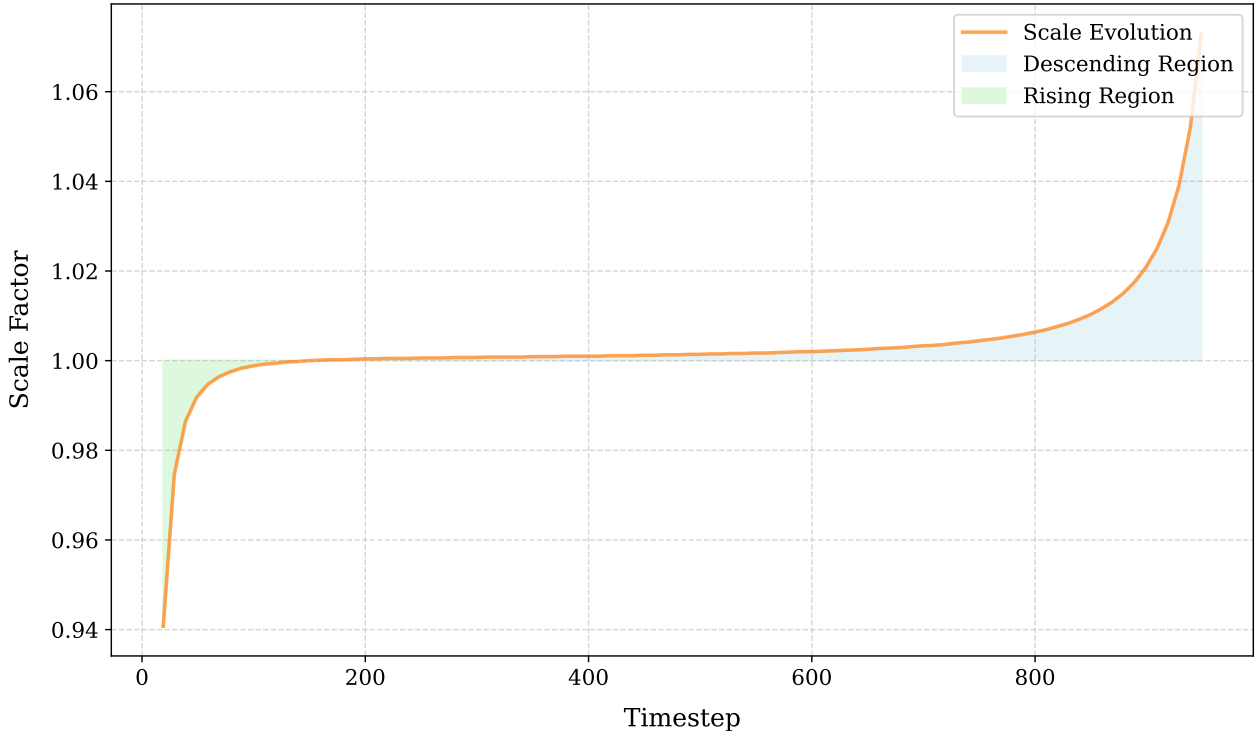
Figure 5: Scale Factor Variation Curve with Timestep During the Diffusion Model Inference Process

3.4 AB-Cache: High-Order Linear Approximation Caching for Accelerated Adams-Bashforth Schemes

In this subsection, we introduce an innovative training-free caching acceleration method designed to minimize prediction inaccuracies caused by caching. By leveraging network output information from the preceding k time steps, this approach extends beyond traditional single-step caching strategies. The method's workflow is illustrated in Fig. 1. Unlike prior techniques that reuse only the immediately preceding time step's network output, we generalize the framework to incorporate information from the preceding k time steps while maintaining a truncation error bound of order $O(h^k)$. To achieve this, we combine the k-th and $(k + 1)$-th order Adams-Bashforth methods, leading to Proposition 2, which encapsulates the core innovation of our approach. By embedding this concept into a standard caching methodology, we derive a comprehensive workflow that balances computational efficiency with predictive accuracy, enabling more robust error control while retaining the efficiency benefits of caching.

Proposition 2. *For $k = 2, 3, 4$, we can show the following k linear recursive relationship of $\hat{\epsilon}_\theta \left(\boldsymbol{x}_{t_\lambda(\lambda_n)}, t_\lambda(\lambda_n) \right)$ and $\hat{\epsilon}_\theta \left(\boldsymbol{x}_{t_\lambda(\lambda_{n-i})}, t_\lambda(\lambda_{n-i}) \right)$ where $1 \leq i \leq k$:*

$$\hat{\epsilon}_\theta \left(\boldsymbol{x}_{t_\lambda(\lambda_n)}, t_\lambda(\lambda_n) \right) = \sum_{i=1}^{k} (-1)^{i+1} \binom{k}{i} e^{ih} \hat{\epsilon}_\theta \left(\boldsymbol{x}_{t_\lambda(\lambda_{n-i})}, t_\lambda(\lambda_{n-i}) \right) + O(h^k). \tag{3.6}$$

Proof. According to the general k-th order Adams-Bashforth scheme in Appendix A, for the following integral,

$$I = \int_{\lambda_{t_n}}^{\lambda_{t_{n+1}}} e^{-\lambda} \hat{\epsilon}_\theta \left(\boldsymbol{x}_{t_\lambda(\lambda)}, t_\lambda(\lambda) \right) \mathrm{d}\lambda,$$

we respectively adopt k-th order and $(k + 1)$-th order Adams-Bashforth scheme to approximate the value of I:

$$I = h \sum_{j=0}^{k-1} b_j^{(k)} e^{-\lambda_{n-j}} \hat{\epsilon}_\theta \left(\boldsymbol{x}_{t_\lambda(\lambda_{n-j})}, t_\lambda(\lambda_{n-j}) \right) + O(h^{k+1}). \tag{3.7}$$

$$I = h \sum_{j=0}^{k} b_j^{(k+1)} e^{-\lambda_{n-j}} \hat{\epsilon}_\theta \left(\boldsymbol{x}_{t_\lambda(\lambda_{n-j})}, t_\lambda(\lambda_{n-j}) \right) + O(h^{k+2}). \tag{3.8}$$

where $b_j^{(k)} (0 \leq j \leq k - 1)$ are the coefficients of k-th order scheme and $b_j^{(k+1)} (0 \leq j \leq k)$ are the coefficients of $(k+1)$-th order scheme. Combining the approximation relationship (3.7) and (3.8), we can get the following linear recursive relationship for $k = 1, 2, 3, 4$ with the known weight coefficients in general Adams-Bashforth method

$$e^{-\lambda_n} \hat{\epsilon}_\theta \left(\boldsymbol{x}_{t_\lambda(\lambda_n)}, t_\lambda(\lambda_n) \right) = \sum_{j=1}^{k-1} \frac{b_j^{(k)} - b_j^{(k+1)}}{b_0^{(k+1)} - b_0^{(k)}} e^{-\lambda_{n-j}} \hat{\epsilon}_\theta \left(\boldsymbol{x}_{t_\lambda(\lambda_{n-j})}, t_\lambda(\lambda_{n-j}) \right)$$

$$- \frac{b_k^{(k+1)}}{b_j^{(k)} - b_j^{(k+1)}} e^{-\lambda_{n-k}} \hat{\epsilon}_\theta \left(\boldsymbol{x}_{t_\lambda(\lambda_{n-k})}, t_\lambda(\lambda_{n-k}) \right) + O(h^k).$$

For $k = 1, 2, 3, 4$, it is easy to check the above relationship is the same as

$$e^{-\lambda_n} \hat{\epsilon}_\theta \left(\boldsymbol{x}_{t_\lambda(\lambda_n)}, t_\lambda(\lambda_n) \right) = \sum_{i=1}^{k} (-1)^{i+1} \binom{k}{i} e^{-\lambda_{n-i}} \hat{\epsilon}_\theta \left(\boldsymbol{x}_{t_\lambda(\lambda_{n-i})}, t_\lambda(\lambda_{n-i}) \right) + O(h^k),$$

which is equivalent to the recursive relationship (3.6). □
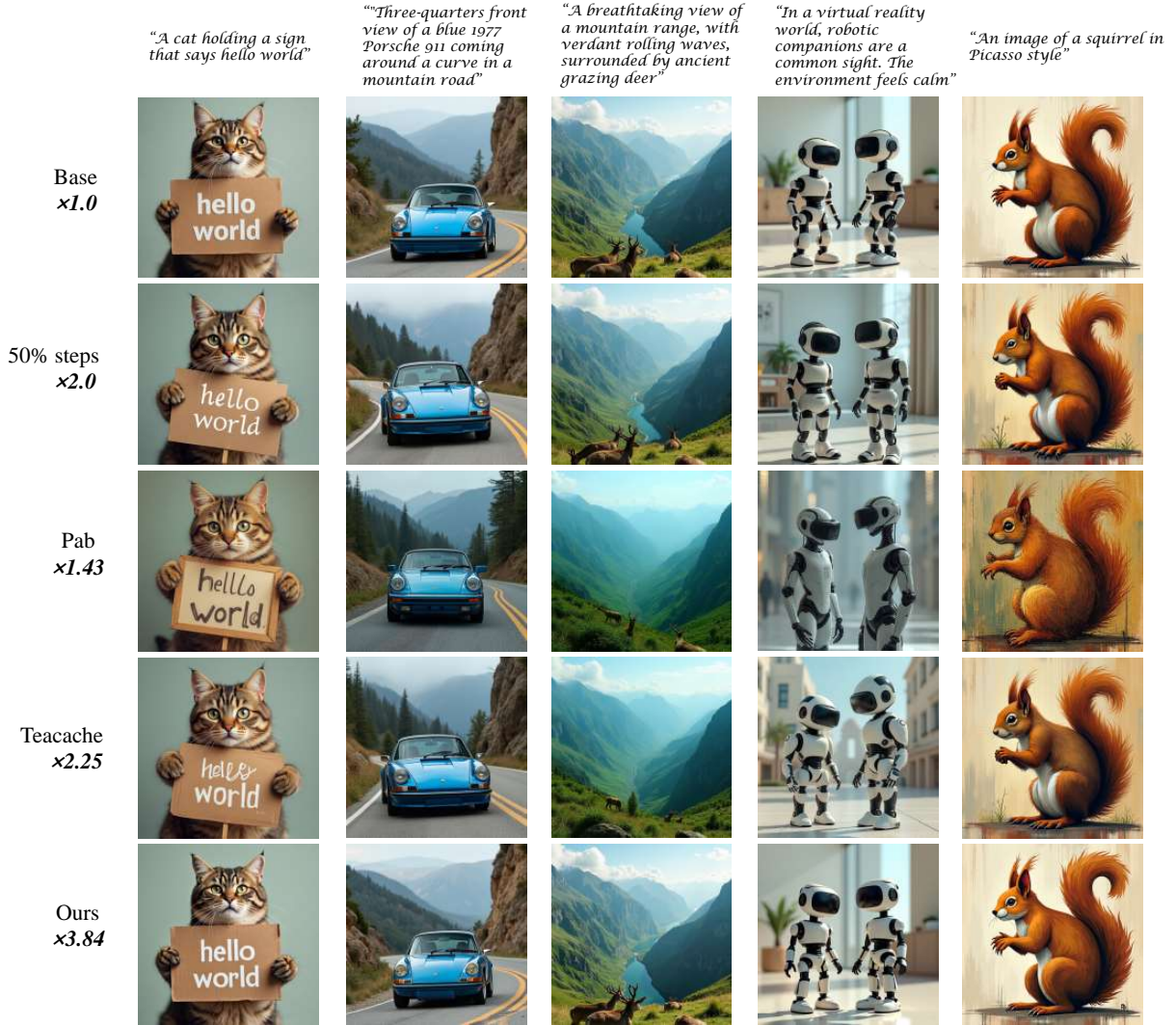
Figure 6: Visualization results for different acceleration methods on FLUX.1-dev model

Remark 1. For general k, we conjecture that the linear recursive relationship (3.6) still holds for $\hat{\epsilon}_\theta \left(\boldsymbol{x}_{t_\lambda(\lambda_{n-i})}, t_\lambda(\lambda_{n-i}) \right)$ where $0 \leq i \leq k$. However, the general weight coefficients $b_j^{(k)}$ $(0 \leq j \leq k-1)$ depend on certain numerical integration (see Appendix A). While proving the general case is challenging, verifying specific instances is straightforward. In practice, we typically do not require higher-order approximations in experiments, so the formula in Proposition 2 is already sufficient for practical purposes. For flow matching, just drop the exponential term in Eq. (3.6).

4 Experiments

4.1 Experimental Setup

To comprehensively evaluate the effectiveness of our proposed acceleration method, we conduct extensive experiments across both image synthesis and video synthesis tasks, benchmarking against state-of-the-art models in each domain.

Model Configurations. In our text-to-video generation study, we compare our approach with
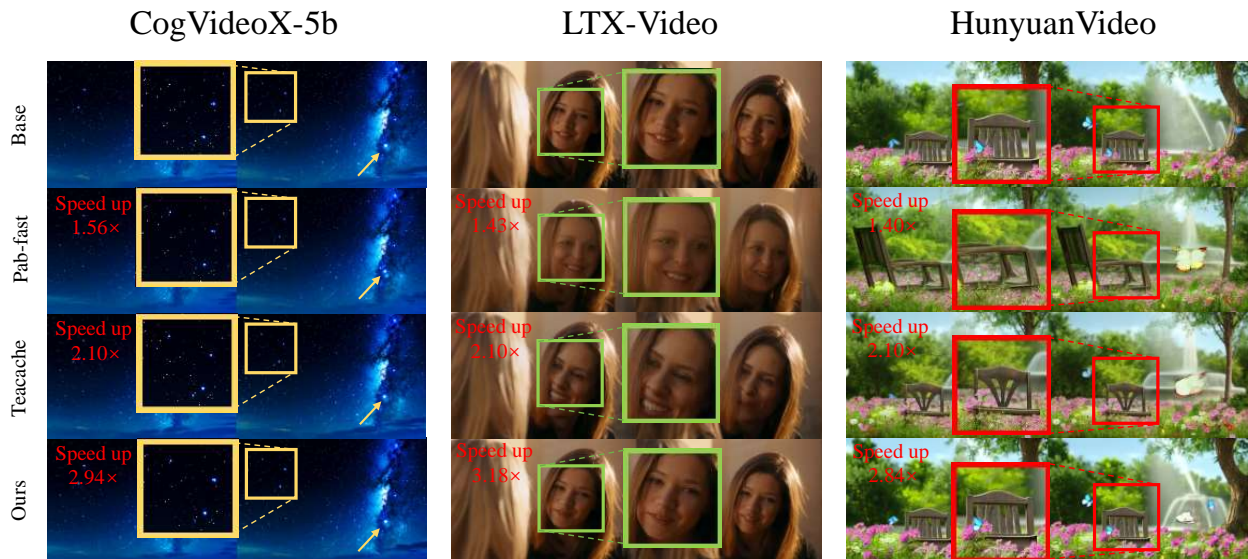
Figure 7: Visual quality comparison between CogVideoX-5b, LTX and HunyuanVideo under different acceleration methods. maintaining high-quality generation without these problems.

three state-of-the-art DiT-based model—HunyuanVideo (Kong et al., 2024), CogVideoX-5B (Yang et al., 2024), and LTX-Video (HaCohen et al., 2024). To ensure fair evaluation while respecting architectural differences, HunyuanVideo and LTX-Video employ the FlowMatchEulerDiscreteScheduler, whereas CogVideoX-5B utilizes the DDIM Scheduler. This configuration allows for systematic performance comparisons while accounting for each model's distinct scheduling mechanisms. For text-to-image generation, we evaluate FLUX.1-dev using a 50-step FlowMatchEulerDiscreteScheduler as the default configuration. All experiments are conducted with NVIDIA L40 48GB GPUs.

Table 1: Quantitative evaluation of inference efficiency and visual quality in video generation models. AB-Cache consistently achieves superior efficiency and better visual quality across different base models, sampling schedulers, video resolutions, and lengths.

Method	Efficiency			Visual Quality			
	FLOPs (PFLOPs) ↓	Speedup ↑	Latency (s) ↓	VBench ↑	LPIPS ↓	SSIM ↑	PSNR ↑
LTX-Video (48 frames, 704×480)							
LTX-Video ($T = 50$)	22.59	1×	5.74	72.99%	-	-	-
50% steps	11.30	2×	2.87	72.86%	0.1985	0.8338	23.08
Δ-DiT	21.93	1.03×	5.54	72.39%	0.6633	0.5448	12.68
PAB-slow	16.49	1.37×	4.19	72.42%	0.2885	0.7851	20.15
PAB-fast	15.80	1.43×	4.01	72.01%	0.3460	0.7445	18.92
Teacache	10.76	2.10×	2.73	72.51%	0.1166	0.8883	26.95
AB-Cache (Order=3)	**7.10**	**3.18** ×	**1.80**	**73.26%**	0.1949	0.8321	22.91
AB-Cache (Order=2)	**7.10**	**3.18** ×	**1.80**	73.18%	**0.1286**	**0.8921**	**27.24**
HunyuanVideo (61 frames, 320×512)							
HunyuanVideo ($T = 50$)	61.32	1×	150.04	79.37%	-	-	-
50% steps	30.66	2.00×	75.02	79.17%	0.1589	0.8077	24.11
Δ-DiT	59.53	1.03×	145.67	77.21%	0.5692	0.4811	11.91
PAB-slow	46.11	1.33×	112.81	77.64%	0.2116	0.6923	20.98
PAB-fast	43.80	1.40×	107.17	76.95%	0.4094	0.5595	17.64
Teacache	29.20	2.10×	71.45	78.46%	0.2142	0.7622	21.78
AB-Cache (Order=3)	**21.59**	**2.84×**	**52.83**	79.26%	**0.1866**	**0.8251**	**25.78**
CogVideoX-T2V-5B (65 frames, 320×512)							
CogVideoX-T2V-5B ($T = 50$)	14.79	1×	144.73	71.43%	-	-	-
50% steps	7.40	2×	72.37	71.22%	0.1583	0.8067	23.68
Δ-DiT	14.50	1.02×	141.89	62.55%	0.5388	0.3736	13.85
PAB-slow	10.88	1.36×	106.42	67.30%	0.3059	0.6550	18.80
PAB-fast	9.48	1.56×	92.78	66.81%	0.5499	0.4717	15.47
Teacache	7.04	2.10×	68.92	71.01%	0.1414	0.8269	24.18
AB-Cache (Order=3)	**5.21**	**2.84×**	**50.96**	71.11%	**0.0538**	**0.8326**	**25.30**

Evaluation Metrics. We evaluate the performance of our method from two key perspectives: **inference efficiency** and **generation quality**. For inference efficiency, we measure FLOPs to

quantify computational complexity and latency (in seconds) to assess real-time inference speed. The evaluation methods for generation quality vary across different tasks, as detailed below:

Text-to-video generation. VBench is a comprehensive benchmark suite designed to systematically evaluate the performance of video generative models across multiple dimensions, including visual quality, temporal coherence, and semantic alignment. We use VBench as the primary metric for evaluating video generation quality. Based on the 946 prompts provided by VBench, each prompt generates five independent videos, resulting in a total of 4,730 videos used to assess the 16 distinct metrics proposed by VBench. Additionally, we incorporate PSNR, LPIPS, and SSIM as supplementary metrics to further assess the quality of generated videos. To ensure a representative evaluation, we randomly sample 200 prompts from the set provided by VBench and use them to compute these metrics, allowing for a more comprehensive analysis of the video generation performance. These settings are consistent with the recent work (Liu et al., 2024b; Zhao et al., 2024), ensuring a fair and comparable evaluation of video generation quality.

Text-to-image generation. We conduct inference on 200 DrawBench (Saharia et al., 2022) prompts to generate images at a resolution of 256×256. The generated samples are then evaluated using ImageReward (Xu et al., 2023) and CLIP Score (Hessel et al., 2021) as key metrics to assess image quality and text alignment. Furthermore, we randomly select 30,000 captions from the COCO-2017 dataset [20] to generate 30,000 images with a resolution of 256×256 to compute the FID-30k metric.

4.2 Main Results

Quantitative Comparison on Text-to-Video Generation. As shown in Table 1, we compare our method with three training-free diffusion inference acceleration approaches—Δ-DiT, PAB, and TeaCache—as well as a step reduction method, with the number of steps set to 50%. To verify the generalizability of our method, we conduct comparisons across multiple base models with different settings. Based on the quantitative comparison results, our method achieves the highest PSNR, LPIPS, and SSIM scores while preserving video quality comparable to the base model without any acceleration techniques. Furthermore, according to VBench metrics, our method achieves the best performance, surpassing Δ-DiT, PAB and Teacache. In evaluating the HunyuanVideo baseline, our method achieves a $2.84\times$ speedup, demonstrating substantial acceleration. In the VBench evaluation, we observe an improvement in visual quality, though there is a slight decline in some dimension metrics. On CogVideoX, our method achieves a $2.84\times$ speedup while maintaining the best PSNR, LPIPS, and SSIM scores. In the comparison with the LTX model, our acceleration method delivering the highest quality at a speedup of $3.18\times$.

Quality Comparison on Text-to-Video Generation. Fig. 7 compares the videos generated by our method with those produced by the original model, PAB, and Teacache, all of which operate with a lower speedup ratio. Under diverse prompts containing portraits, objects, and complex environments, our method demonstrates superior performance in: (i) preserving consistent facial details across frames, (ii) maintaining structural stability of foreground objects (e.g., chairs), and (iii) ensuring temporal coherence in background elements (e.g., star fields). The results demonstrate that our generation method effectively maintains the quality and details of the output while achieving faster speed, outperforming the comparison methods.

Quantitative Comparison on Text-to-image Generation. In terms of generation quality, our method achieves the best $3.18\times$ speedup while maintaining the highest generation quality, as evidenced by the FID-30k score and ImageReward metric on the DrawBench, with almost no loss in quality compared to the original non-accelerated approach. Specifically, our method achieves a $3.18\times$ speedup while preserving superior generation quality, as evidenced by an ImageReward

score of 0.7893, which exceeds the base model's score of 0.7717. Regarding semantic alignment, our method achieves the best CLIP score under faster acceleration, demonstrating superior performance in alignment with the text prompts.
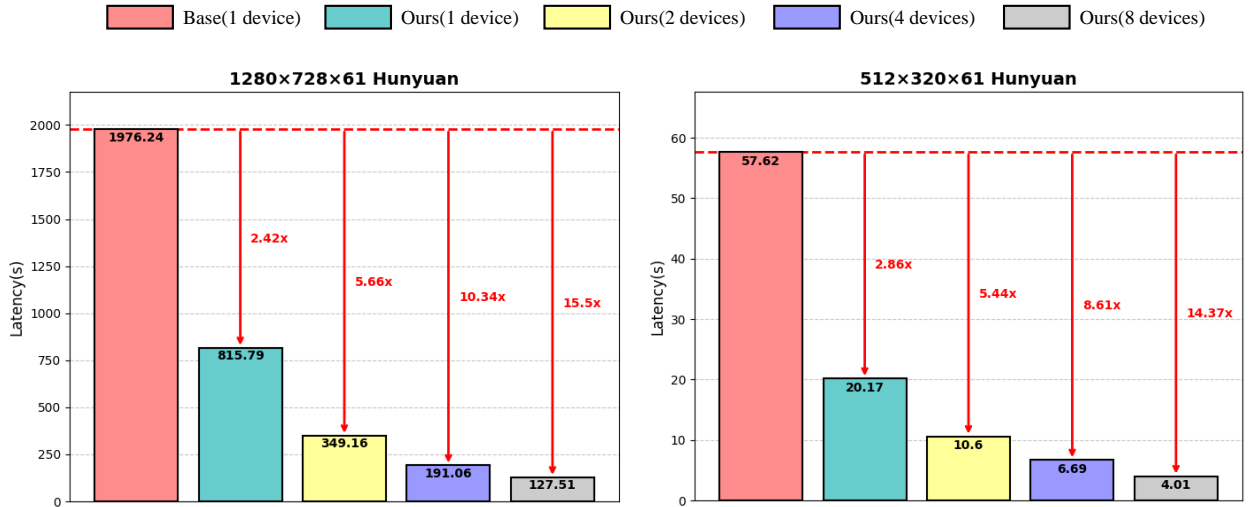
Figure 8: Evaluation of acceleration and scalability of our method in generating larger videos under single- and multi-GPU configurations.

Quality Comparison on Text-to-image Generation. In the qualitative comparison, we generate images using three representative prompts under identical settings across all methods. As shown in Fig. 6, our approach consistently produces the highest visual quality. The figure contrasts results from our method with those from the original model, PAB, and TeaCache, all of which exhibit lower speedup ratios. Under diverse prompts involving text, vehicles, and natural landscapes, our method demonstrates superior performance in: (i) preserving the clarity and legibility of fonts, (ii) maintaining the structural consistency of objects, such as the front-facing orientation of the car, (iii) retaining fine-grained foreground details, such as the deer in the mountain scene, and (iv) ensuring rich, vibrant color fidelity throughout the generated images. The results demonstrate that our generation method effectively maintains the quality and details of the output while achieving faster speed, outperforming the comparison methods.

4.3 Ablation Studies

We conduct ablation studies on the LTX model to evaluate the effectiveness of our proposed method. Our ablation studies on the LTX model primarily investigate: (1) the impact of order (e.g., 1st-order vs. 3rd-order approximations) on generation quality and computational efficiency, (2) scaling behavior across varying frame lengths, resolutions, and GPU configurations.

Quality-Efficiency trade-off of Order. Table 3 demonstrates how varying approximation orders affect generation quality under the same experimental setup, consistent with our theoretical analysis that higher-order approximations reduce error. Importantly, we observe a substantial enhancement in aesthetic quality with increasing approximation order.

Scaling Study. To validate the scalability of our method, we evaluated its performance on HunyuanVideo under different video lengths, resolutions, and GPU configurations. As shown in Figure 8, our acceleration approach maintains consistent generation quality across varying computational scales and multi-GPU settings.

Table 2: Performance comparison of different methods in terms of efficiency and visual quality.

Method	Efficiency			Visual Quality		
	Speedup↑	Latency↓	FLOPS↓ (T)	ImageReward↑	CLIP↑	FID↓
FLUX-1.dev	1.00×	18.90	243.66	77.17	25.55	34.46
50%-step	2.00×	9.45	121.83	76.32	25.31	35.20
PAB	1.43×	13.22	170.39	72.39	25.59	34.14
Teacache	2.25×	8.40	108.29	75.34	25.66	32.85
AB-Cache (Order=2)	**3.10×**	**6.10**	**78.6**	**78.93**	**25.73**	**32.12**

Table 3: Comparison of different orders in terms of Quality Score, Semantic Score, and VBench Score.

Order	Quality Score↑	Semantic Score↑	VBench Score↑
LTX-Video	78.29	51.78	72.99
First-order	77.29	48.35	71.50
2nd-order	78.33	50.98	73.18
3rd-order	**78.79**	51.13	**73.26**

5 Conclusion

In this work, we present a theoretically grounded acceleration method for diffusion models by leveraging the k-th order Adams-Bashforth numerical integration to establish a principled relationship between consecutive denoising steps. Our analysis reveals the U-shaped similarity pattern in adjacent outputs and provides a rigorous truncation error bound of $O(h^k)$, ensuring stable and high-quality generation. The proposed high-order caching mechanism enables a nearly $3\times$ speedup in inference while maintaining performance parity with the base diffusion model, as validated across diverse architectures and tasks (image and video generation). Unlike heuristic reuse strategies, our method offers provable efficiency gains without compromising sample quality. This work bridges the gap between theoretical analysis and practical acceleration in diffusion models, paving the way for real-time applications.

References

Yash Bhalgat, Jinwon Lee, Markus Nagel, Tijmen Blankevoort, and Nojun Kwak. 2020. Lsq+: Improving low-bit quantization through learnable offsets and better initialization. In *Proceedings of the IEEE/CVF conference on computer vision and pattern recognition workshops*. 696–697.

John Charles Butcher. 2016. *Numerical methods for ordinary differential equations*. John Wiley & Sons.

Junsong Chen, Jincheng Yu, Chongjian Ge, Lewei Yao, Enze Xie, Yue Wu, Zhongdao Wang, James Kwok, Ping Luo, Huchuan Lu, et al. 2023. Pixart-α: Fast training of diffusion transformer for photorealistic text-to-image synthesis. *arXiv preprint arXiv:2310.00426* (2023).

Pengtao Chen, Mingzhu Shen, Peng Ye, Jianjian Cao, Chongjun Tu, Christos-Savvas Bouganis, Yiren

Zhao, and Tao Chen. 2024. Δ-DiT: A Training-Free Acceleration Method Tailored for Diffusion Transformers. *arXiv preprint arXiv:2406.01125* (2024).

Xin Dong, Shangyu Chen, and Sinno Pan. 2017. Learning to prune deep neural networks via layer-wise optimal brain surgeon. *Advances in neural information processing systems* 30 (2017).

Zhengyang Geng, Ashwini Pokle, and J Zico Kolter. 2023. One-step diffusion distillation via deep equilibrium models. *Advances in Neural Information Processing Systems* 36 (2023), 41914–41931.

Shuyang Gu, Dong Chen, Jianmin Bao, Fang Wen, Bo Zhang, Dongdong Chen, Lu Yuan, and Baining Guo. 2022. Vector quantized diffusion model for text-to-image synthesis. In *Proceedings of the IEEE/CVF conference on computer vision and pattern recognition*. 10696–10706.

Yoav HaCohen, Nisan Chiprut, Benny Brazowski, Daniel Shalem, Dudu Moshe, Eitan Richardson, Eran Levin, Guy Shiran, Nir Zabari, Ori Gordon, et al. 2024. Ltx-video: Realtime video latent diffusion. *arXiv preprint arXiv:2501.00103* (2024).

Ernst Hairer. 1993. SP N rsett, and G. Wanner. Solving ordinary differential equations I, Nonsti problems.

Jack Hessel, Ari Holtzman, Maxwell Forbes, Ronan Le Bras, and Yejin Choi. 2021. Clipscore: A reference-free evaluation metric for image captioning. *arXiv preprint arXiv:2104.08718* (2021).

Jonathan Ho, Ajay Jain, and Pieter Abbeel. 2020. Denoising diffusion probabilistic models. *Advances in neural information processing systems* 33 (2020), 6840–6851.

Tero Karras, Miika Aittala, Timo Aila, and Samuli Laine. 2022. Elucidating the design space of diffusion-based generative models. *Advances in neural information processing systems* 35 (2022), 26565–26577.

Bo-Kyeong Kim, Hyoung-Kyu Song, Thibault Castells, and Shinkook Choi. 2023. On architectural compression of text-to-image diffusion models. (2023).

Weijie Kong, Qi Tian, Zijian Zhang, Rox Min, Zuozhuo Dai, Jin Zhou, Jiangfeng Xiong, Xin Li, Bo Wu, Jianwei Zhang, et al. 2024. Hunyuanvideo: A systematic framework for large video generative models. *arXiv preprint arXiv:2412.03603* (2024).

Namhoon Lee, Thalaiyasingam Ajanthan, Stephen Gould, and Philip HS Torr. 2019. A signal propagation perspective for pruning neural networks at initialization. *arXiv preprint arXiv:1906.06307* (2019).

Lijiang Li, Huixia Li, Xiawu Zheng, Jie Wu, Xuefeng Xiao, Rui Wang, Min Zheng, Xin Pan, Fei Chao, and Rongrong Ji. 2023b. Autodiffusion: Training-free optimization of time steps and architectures for automated diffusion model acceleration. In *Proceedings of the IEEE/CVF International Conference on Computer Vision*. 7105–7114.

Senmao Li, Taihang Hu, Fahad Shahbaz Khan, Linxuan Li, Shiqi Yang, Yaxing Wang, Ming-Ming Cheng, and Jian Yang. 2023a. Faster diffusion: Rethinking the role of unet encoder in diffusion models. *CoRR* (2023).

Xiuyu Li, Yijiang Liu, Long Lian, Huanrui Yang, Zhen Dong, Daniel Kang, Shanghang Zhang, and Kurt Keutzer. 2023c. Q-diffusion: Quantizing diffusion models. In *Proceedings of the IEEE/CVF International Conference on Computer Vision*. 17535–17545.

Enshu Liu, Xuefei Ning, Zinan Lin, Huazhong Yang, and Yu Wang. 2023a. Oms-dpm: Optimizing the model schedule for diffusion probabilistic models. In *International Conference on Machine Learning*. PMLR, 21915–21936.

Feng Liu, Shiwei Zhang, Xiaofeng Wang, Yujie Wei, Haonan Qiu, Yuzhong Zhao, Yingya Zhang, Qixiang Ye, and Fang Wan. 2024b. Timestep Embedding Tells: It's Time to Cache for Video Diffusion Model. *arXiv preprint arXiv:2411.19108* (2024).

Haohe Liu, Yi Yuan, Xubo Liu, Xinhao Mei, Qiuqiang Kong, Qiao Tian, Yuping Wang, Wenwu Wang, Yuxuan Wang, and Mark D Plumbley. 2024a. Audioldm 2: Learning holistic audio generation with self-supervised pretraining. *IEEE/ACM Transactions on Audio, Speech, and Language Processing* (2024).

Liyang Liu, Shilong Zhang, Zhanghui Kuang, Aojun Zhou, Jing-Hao Xue, Xinjiang Wang, Yimin Chen, Wenming Yang, Qingmin Liao, and Wayne Zhang. 2021. Group fisher pruning for practical network compression. In *International Conference on Machine Learning*. PMLR, 7021–7032.

Xingchao Liu, Xiwen Zhang, Jianzhu Ma, Jian Peng, et al. 2023b. Instaflow: One step is enough for high-quality diffusion-based text-to-image generation. In *The Twelfth International Conference on Learning Representations*.

Cheng Lu, Yuhao Zhou, Fan Bao, Jianfei Chen, Chongxuan Li, and Jun Zhu. 2022a. Dpm-solver: A fast ode solver for diffusion probabilistic model sampling in around 10 steps. *Advances in Neural Information Processing Systems* 35 (2022), 5775–5787.

Cheng Lu, Yuhao Zhou, Fan Bao, Jianfei Chen, Chongxuan Li, and Jun Zhu. 2022b. Dpm-solver++: Fast solver for guided sampling of diffusion probabilistic models. *arXiv preprint arXiv:2211.01095* (2022).

Zhengyao Lv, Chenyang Si, Junhao Song, Zhenyu Yang, Yu Qiao, Ziwei Liu, and Kwan-Yee K Wong. 2024. Fastercache: Training-free video diffusion model acceleration with high quality. *arXiv preprint arXiv:2410.19355* (2024).

Xinyin Ma, Gongfan Fang, and Xinchao Wang. 2024a. Deepcache: Accelerating diffusion models for free. In *Proceedings of the IEEE/CVF conference on computer vision and pattern recognition*. 15762–15772.

Xin Ma, Yaohui Wang, Gengyun Jia, Xinyuan Chen, Ziwei Liu, Yuan-Fang Li, Cunjian Chen, and Yu Qiao. 2024b. Latte: Latent diffusion transformer for video generation. *arXiv preprint arXiv:2401.03048* (2024).

Chenlin Meng, Robin Rombach, Ruiqi Gao, Diederik Kingma, Stefano Ermon, Jonathan Ho, and Tim Salimans. 2023. On distillation of guided diffusion models. In *Proceedings of the IEEE/CVF Conference on Computer Vision and Pattern Recognition*. 14297–14306.

William Peebles and Saining Xie. 2023. Scalable diffusion models with transformers. In *Proceedings of the IEEE/CVF international conference on computer vision*. 4195–4205.

Aditya Ramesh, Prafulla Dhariwal, Alex Nichol, Casey Chu, and Mark Chen. 2022. Hierarchical text-conditional image generation with clip latents. *arXiv preprint arXiv:2204.06125* 1, 2 (2022), 3.

Robin Rombach, Andreas Blattmann, Dominik Lorenz, Patrick Esser, and Björn Ommer. 2022. High-resolution image synthesis with latent diffusion models. In *Proceedings of the IEEE/CVF conference on computer vision and pattern recognition*. 10684–10695.

Olaf Ronneberger, Philipp Fischer, and Thomas Brox. 2015. U-net: Convolutional networks for biomedical image segmentation. In *Medical image computing and computer-assisted intervention–MICCAI 2015: 18th international conference, Munich, Germany, October 5-9, 2015, proceedings, part III 18*. Springer, 234–241.

Chitwan Saharia, William Chan, Saurabh Saxena, Lala Li, Jay Whang, Emily L Denton, Kamyar Ghasemipour, Raphael Gontijo Lopes, Burcu Karagol Ayan, Tim Salimans, et al. 2022. Photo-realistic text-to-image diffusion models with deep language understanding. *Advances in neural information processing systems* 35 (2022), 36479–36494.

Tim Salimans and Jonathan Ho. 2022. Progressive distillation for fast sampling of diffusion models. *arXiv preprint arXiv:2202.00512* (2022).

Axel Sauer, Dominik Lorenz, Andreas Blattmann, and Robin Rombach. 2024. Adversarial diffusion distillation. In *European Conference on Computer Vision*. Springer, 87–103.

Yuzhang Shang, Zhihang Yuan, Bin Xie, Bingzhe Wu, and Yan Yan. 2023. Post-training quantization on diffusion models. In *Proceedings of the IEEE/CVF conference on computer vision and pattern recognition*. 1972–1981.

Xuan Shen, Zhao Song, Yufa Zhou, Bo Chen, Yanyu Li, Yifan Gong, Kai Zhang, Hao Tan, Jason Kuen, Henghui Ding, et al. 2024. Lazydit: Lazy learning for the acceleration of diffusion transformers. *arXiv preprint arXiv:2412.12444* (2024).

Jiaming Song, Chenlin Meng, and Stefano Ermon. 2020a. Denoising diffusion implicit models. *arXiv preprint arXiv:2010.02502* (2020).

Yang Song, Prafulla Dhariwal, Mark Chen, and Ilya Sutskever. 2023. Consistency models. (2023).

Yang Song, Conor Durkan, Iain Murray, and Stefano Ermon. 2021. Maximum likelihood training of score-based diffusion models. *Advances in neural information processing systems* 34 (2021), 1415–1428.

Yang Song and Stefano Ermon. 2019. Generative modeling by estimating gradients of the data distribution. *Advances in neural information processing systems* 32 (2019).

Yang Song, Jascha Sohl-Dickstein, Diederik P Kingma, Abhishek Kumar, Stefano Ermon, and Ben Poole. 2020b. Score-based generative modeling through stochastic differential equations. *arXiv preprint arXiv:2011.13456* (2020).

Zeyue Tian, Yizhu Jin, Zhaoyang Liu, Ruibin Yuan, Xu Tan, Qifeng Chen, Wei Xue, and Yike Guo. 2025. AudioX: Diffusion Transformer for Anything-to-Audio Generation. *arXiv preprint arXiv:2503.10522* (2025).

Ashish Vaswani, Noam Shazeer, Niki Parmar, Jakob Uszkoreit, Llion Jones, Aidan N Gomez, Łukasz Kaiser, and Illia Polosukhin. 2017. Attention is all you need. *Advances in neural information processing systems* 30 (2017).

Jiazheng Xu, Xiao Liu, Yuchen Wu, Yuxuan Tong, Qinkai Li, Ming Ding, Jie Tang, and Yuxiao Dong. 2023. Imagereward: Learning and evaluating human preferences for text-to-image generation. *Advances in Neural Information Processing Systems* 36 (2023), 15903–15935.

Zhuoyi Yang, Jiayan Teng, Wendi Zheng, Ming Ding, Shiyu Huang, Jiazheng Xu, Yuanming Yang, Wenyi Hong, Xiaohan Zhang, Guanyu Feng, et al. 2024. Cogvideox: Text-to-video diffusion models with an expert transformer. *arXiv preprint arXiv:2408.06072* (2024).

Wentian Zhang, Haozhe Liu, Jinheng Xie, Francesco Faccio, Mike Zheng Shou, and Jürgen Schmidhuber. 2024. Cross-attention makes inference cumbersome in text-to-image diffusion models. *arXiv e-prints* (2024), arXiv–2404.

Xuanlei Zhao, Xiaolong Jin, Kai Wang, and Yang You. 2024. Real-time video generation with pyramid attention broadcast. *arXiv preprint arXiv:2408.12588* (2024).

Zangwei Zheng, Xiangyu Peng, Tianji Yang, Chenhui Shen, Shenggui Li, Hongxin Liu, Yukun Zhou, Tianyi Li, and Yang You. 2024. Open-sora: Democratizing efficient video production for all. *arXiv preprint arXiv:2412.20404* (2024).

A k-th Order Adams-Bashforth Scheme

We can adopt the general k-th order Adams-Bashforth scheme to obtain a more accurate value of I. For simplicity, we use notation t_k instead of λ_{t_k} and $f(\tau) := e^{-\tau} \hat{\boldsymbol{\epsilon}}_\theta \left(\boldsymbol{x}_{t_\lambda(\tau)}, t_\lambda(\tau) \right)$, our goal is to get the integral of $f(\tau)$ over the interval $[t_n, t_{n+1}]$, thus:

$$I = \int_{t_n}^{t_{n+1}} f(\tau) \, d\tau.$$

According to the standrad k-th order Adams-Bashforth scheme, we need k previous time steps $t_{n-k+1}, t_{n-k+2}, \ldots, t_n$ (with uniform step size h). We construct a $(k-1)$ degree Lagrange interpolating polynomial $p(\tau)$ that satisfies:

$$p(t_{n-j}) = f(t_{n-j}), \quad j = 0, 1, \ldots, k - 1.$$

Introduce the normalized variable $s = \frac{\tau - t_n}{h}$, mapping the interpolation points to $s = -(k-1), -(k-2), \cdots, 0$. The polynomial becomes:

$$p(s) = \sum_{j=0}^{k-1} f(t_{n-j}) \cdot L_j(s),$$

where $L_j(s)$ $(0 \le j \le k - 1)$ are Lagrange basis polynomials:

$$L_j(s) = \prod_{\substack{m=0 \\ m \ne j}}^{k-1} \frac{s + m}{-j + m}.$$

Substitute $p(\tau)$ into the integral and change variables to s:

$$\int_{t_n}^{t_{n+1}} p(\tau) \, d\tau = h \int_0^1 p(s) \, ds = h \sum_{j=0}^{k-1} \left(f(t_{n-j}) \int_0^1 L_j(s) \, ds \right).$$

Define the integration weights b_j as:

$$b_j = \int_0^1 L_j(s) \, ds.$$

The integral I can be approximated by $h \sum_{j=0}^{k-1} b_j f(t_{n-j})$ with local truncation error $O(h^{k+1})$ and global truncation error $O(h^k)$. The weights b_j depend only on k and are precomputed via integration of the basis polynomials. For example, for $k = 3$ (3rd order method), the basis polynomials are:

$$L_0(s) = \frac{(s+1)(s+2)}{2}, \quad L_1(s) = -\frac{s(s+2)}{1}, \quad L_2(s) = \frac{s(s+1)}{2},$$

and the coefficients for are derived as:

$$b_0 = \frac{23}{12}, \quad b_1 = -\frac{4}{3}, \quad b_2 = \frac{5}{12}.$$

Common coefficients $k = 1$ to 5 are presented in Table 4.

Table 4: Weight Coefficients

Order k	b_0	b_1	b_2	b_3	b_4
1	1				
2	$\frac{3}{2}$	$-\frac{1}{2}$			
3	$\frac{23}{12}$	$-\frac{4}{3}$	$\frac{5}{12}$		
4	$\frac{55}{24}$	$-\frac{59}{24}$	$\frac{37}{24}$	$-\frac{3}{8}$	
5	$\frac{1901}{720}$	$-\frac{2774}{720}$	$\frac{2616}{720}$	$-\frac{1274}{720}$	$\frac{251}{720}$